Macromol. Symp. 139, 13–30 (1999)

Interfacial Phenomena, Adhesion and Macroscopic Properties in Polymer Composites

M. Pegoraro*, L. Di Landro, F. Severini
Dipartimento di Chimica Industriale e Ingegneria Chimica "G. Natta", Politecnico di Milano, Piazza L. da Vinci 32, 20133 Milano, Italy

Abstract: The microfragmentation or the single-fiber composite method for the evaluation of fiber-matrix adhesion in polymer composites is presented emphasizing advantages and drawbacks. The improvements of the methods introduced in recent years (laser Raman spectroscopy, optical examination of interfacial region, estimation of the stress state at the interface, consideration of viscoelastic properties of the matrix) to obtain more detailed information on the interface failure mechanisms are described. A modified method with a coaxial geometry, which extends the applicability of the test to brittle matrices, is shown. A number of experimental results obtained both with thermoplastic and thermoset matrices containing carbon and glass fibers is reported. Chemical modifications of carbon fiber surfaces were carried out, which effectively changed the adhesion to the high-performance bismaleimide matrix. In particular, the treatment with ammonia is shown to be promising for improvement of adhesion in graphite/bismaleimide composites.

INTRODUCTION

Evaluation of adhesion between polymer matrices and reinforcing inclusions is of remarkable importance in the study of the mechanical behaviour of composite materials. The inclusion/matrix interface is a critical area in determining the composite properties. The importance of the interface is strongly dependent on the chemical nature of the components, on the loading conditions and on the inclusion geometry. Therefore different techniques should be employed for inclusions with the aspect ratio of unity (spheres) and higher (fibers).

Several test methods were developed for measuring adhesion using single fibers or groups of fibers. In the last years three basic methods have been mainly used: fiber pull-out, fiber fragmentation, and fiber microcompression (indentation) [1]. The single-fiber fragmentation is particularly interesting because the state of stress produced on the single fiber is more similar to the state of stress present in a composite than in the other two methods mentioned. Moreover, in transparent polymer matrices it is possible to determine, in transmitted polarized light, the mode and the locus of failure.

We used this method in evaluating the fiber-matrix interfacial adhesion, particularly in polymers with good high-temperature performance, both thermosets and thermoplastics, such as bismaleimide (BMI), epoxy resin, polyetheretherketone (PEEK), polyetherimide (PEI-ULTEM), polyethersulfone (PES), poly(ethylene terephthalate) (PET), polypropylene (PP) [2-6]. We will discuss the main fundamental aspects and the new improvements which make the single-fiber composite (SFC) test one of the most powerful practical methods for the adhesion studies.

Microfragmentation or single-fiber composite test

It is known that a reinforcing effect can be obtained only if the volume fraction of fibers is higher than a minimum value (V_{min}) [7]. Below this value, the fibers break during a tensile test at small elongations without a failure of the whole composite. Let us consider a single

© WILEY-VCH Verlag GmbH, D-69469 Weinheim, 1999 CCC 1022-1360/99/$ 17.50+.50/0

fiber of diameter d, immersed in a matrix, keeping its volume fraction lower than V_{min}. Under axial load the fiber equilibrium equation gives

$$\tau^{*}(\pi d)\,\mathrm{d}x=\left(\frac{\pi d^{2}}{4}\right)\mathrm{d}\sigma_{f} \tag{1}$$

and

$$\tau^{*}=\frac{d}{4}\frac{\mathrm{d}\sigma_{f}}{\mathrm{d}x} \tag{2}$$

where σ_f is the fiber stress and τ is the local shear stress at the fiber surface over a length dx. A theoretical elastic model of the stress σ along a fiber immersed in a polymer and τ at its interface, imposed by an external axial load, was proposed by Cox [8].

As the external load is increased, τ may reach the yielding shear stress of the matrix (τ_y) beginning at the fiber ends in the case of very good adhesion, or reach the maximum interface adhesion shear stress (τ_{ad}) if the latter is lower than the matrix yield shear stress (Fig. 1a). Another failure mode is the frictional debonding.

Whatever the mode, a τ limit (τ_l) is assumed to be reached. On increasing strain, a further increase in σ_f is possible because a larger interfacial area at constant τ is involved by the shear phenomena (Fig. 1b) until the fiber strength value σ_{bf} is reached. Fiber failure occurs at or beyond a length defined as semicritical length $l_c/2$ (Fig. 1c). For the fiber length lower than l_c, the tensile strength of the fiber cannot be reached. By integration of Eq. (2) for constant τ, we get the interfacial shear strength (IFSS) expression for τ_{ad}

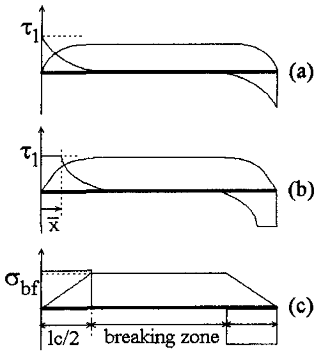

Fig. 1 Stress distribution along a fiber fragment embedded in a matrix

$$\tau_{ad}=\frac{\sigma_{bf}d}{2l_c} \tag{3}$$

The fiber fragmentation will continue until each fragment is reduced to a length $l \le l_c$. In conclusion, the fiber will break into fragments of length between $l_c/2$ (minimum) and l_c (maximum), i.e. the average fragment length l will be

$$\bar{l}=\frac{3l_c}{4} \tag{4}$$

The lengths of the fragments are measured by the nonius of an optical microscope.

Figure 2 shows, for example, the fragment length distribution $P(l)$ of carbon fibers embedded in polyetherimide (PEI) and epoxy matrix. The mean fragment length $\bar{l}$ is calculated in correspondence of $P = 0.5$; l_c and $_{ad}$ are calculated using Eqs. 3 and 4.

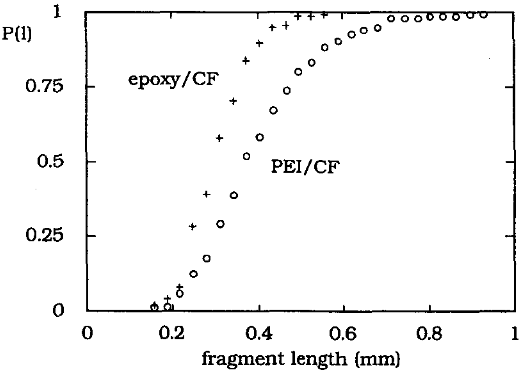

Fig. 2
Examples of fragment length distributions in SFC tests

Table 1 reports a series of results obtained by us in a number of fiber/matrix systems; τ_{ad} values were calculated using σ_{bf} values obtained as in the following.

The actual strength of brittle fibers is distributed on their length over a relatively wide range, the experimental distribution of the fragment lengths being wider than in the case when σ_{bf} is constant along the fiber. l_c depends both on the mean value of σ_{bf} and on its distribution.

Table 1 Adhesion parameters of matrix/fiber systems

Matrix/fiber system	l_c (mm)	τ (MPa)
PEEK/carbon (HTA, XAS)	0.52	37.3-39
PEI/ carbon (HTA, XAS)	0.55-0.5	35-40
PES/carbon (HTA)	0.76	23.5
PP/glass	3.02	3.75
Epoxy (Shell Epon828)/carbon (AS4)	0.5	47.9
Epoxy (Shell Epon828)/graphite (HMS4)	0.52	40.3
Epoxy (DGEBA-IPDA/carbon (XAS)	0.63	36
Epoxy (Ciba LY556-HT972)/carbon (T800)	0.41	45.7
Epoxy (Ciba LY556-HT972)/graphite (M40)	0.41	31
Epoxy (Ciba LY556-HT972)-BMI/T800	0.43	38.5
Epoxy (Ciba LY556-HT972)-BMI/M40	0.70	17.5
Toughened epoxy (DGEBA-IPDA+2.5% CTBN)/XAS	4.5	5
Epoxy (DGEBA-IPDA)/glass	0.5	56
Toughened epoxy (DGEBA-IPDA+2.5% CTBN)/glass	1.3	12

HTA - Toho Rayon, XAS - Courtalds, T800, M40 - Toray, AS4, HMS4 - Hercules

The tensile strength of brittle fibers such as carbon and glass fibers, behaves according to the Weibull distribution function [9]. The failure probability $P(\sigma)$ of a fiber for stresses lower than σ is expressed as

$$P(\sigma) = 1 - \exp\left[-l\left(\frac{\sigma}{\beta}\right)^{\alpha}\right] \qquad (5)$$

and the mean fiber strength $\bar{\sigma}$ of a large number of fibers is [5]

$$\bar{\sigma} = \frac{\beta}{l^{1/\alpha}}\Gamma\left(\frac{\alpha+1}{\alpha}\right) \tag{6}$$

where l is the fiber length, α and β are the Weibull parameters and Γ is the complete gamma function.

A number of adhesion studies was done by many authors, following the microfragmentation procedure [10]. It was found that the proposed method gives rather reproducible results, which are useful for comparative and practical uses. Its employment is especially important when surface modifications or different sizing agents have to be studied.

The SFC method presents a number of theoretical and practical difficulties. In fact it always assumes an elastoplastic behaviour of the matrix and/or of the interface and the presence of a constant τ in correspondence of the fiber breaks even when failure happens by a mixed failure mode. Moreover, it is not able to put in evidence the thermodynamically reversible work of adhesion because of the irreversible mechanical dissipations. The Kelly-Tyson model is not able to distinguish friction effects during debonding from the elastoplastic shear in the bonded zone. During a fragmentation test, in the debonded zone, τ depends on pressure only ($\tau = \mu p$ where μ is the friction coefficient and p is the radial stress at the fiber surface). In the actual situation, the shear stress is not equal for all the interface failure mechanisms; therefore the maximum adhesion stress τ_{max} is greater than the mean stress τ estimated according to the Kelly-Tyson procedure. Another practical limitation is that the test can be applied to matrices characterized by ultimate strains equal at least 2÷3 times the fiber break strain ε_{bf}. This is needed to reach saturation in the fragmentation process.

The τ_{ad} appears to be a phenomenological parameter rather than a well founded absolute measure of the adhesion. However, many efforts are currently done to try to put in evidence separately the different physical and chemical factors which influence τ_{ad} and to express quantitatively these contributions.

The last main improvements are:

(i) the direct method of fiber strain measurement;

(ii) the examination of the failure types in the SFC tests and the study of the corresponding energies needed for failure;

(iii) the study of the viscoelastic behaviour of the matrix which rules the pressure at the interface and the debonding.

In the following we present some considerations on these new aspects of the SFC test.

Direct method of fiber strain measurement

A very important method for measuring the interfacial shear strength (IFSS) is nowadays the laser Raman spectroscopy (LRS) [11]. It is capable of measuring the strain ε of the fiber immersed in a polymer matrix in each point of the fiber, when submitted to an external load. In this way, the stress σ present in the fiber can be evaluated by $\sigma = E\varepsilon$. The elastic modulus E must be obviously found with the fiber alone by preliminary tensile tests.

Carbon fibers (but not glass fibers) are suitable for strain analysis by Raman laser spectroscopy. They exhibit three distinct bands in the Raman spectrum. In the first-order region, up to 1800 cm^{-1}, scattering effects are found at about 1350 cm^{-1} (D line) attributed to vibrations induced by disorder and at 1580 cm^{-1} (G line) attributed to E_{2g} in-plane vibration of the graphitic cell; in the second-order region, the band around 2700 cm^{-1} (G' line) is associated with the three-dimensional crystallinity and is related to the 1350 cm^{-1} vibration. Low-modulus high-tenacity fibers (such as T800) are less crystalline than high-modulus fibers (such as M40) and present broader Raman D and G bands not exhibiting the G' line. The G line is normally used for strain analysis, being particularly reliable for crystalline high-modulus fibers. Raman frequency of the G peak was found to shift in a regular proportional way towards lower frequency values by increasing tensile strain. A linear correspondence between Raman frequency shift (cm^{-1}) and strain is found by calibration [12]. The spatial resolution of LRS is of the order of 1 μm. Confocal Raman microscopy allows to obtain the spectrum of the carbon fiber embedded in a resin.

When the single-fiber composite sample is submitted to a tensile experiment, microfragmentation is developed and each broken segment end becomes a place of stress variation at the ends from 0 to the σ_f. The elementary force balance equation Eq. (1) allows to express the local shear stress acting on the fiber in the place x at the interface (ISS) as

$$\tau(x) = E_f \frac{r_0}{2} \frac{d\varepsilon(x)}{dx} \qquad (7)$$

Therefore the Raman method allows to measure for the first time the axial stress and the shear stress distribution in the proximity of each segment end directly and not only by using mathematical models (such as that of Kelly and Cox).

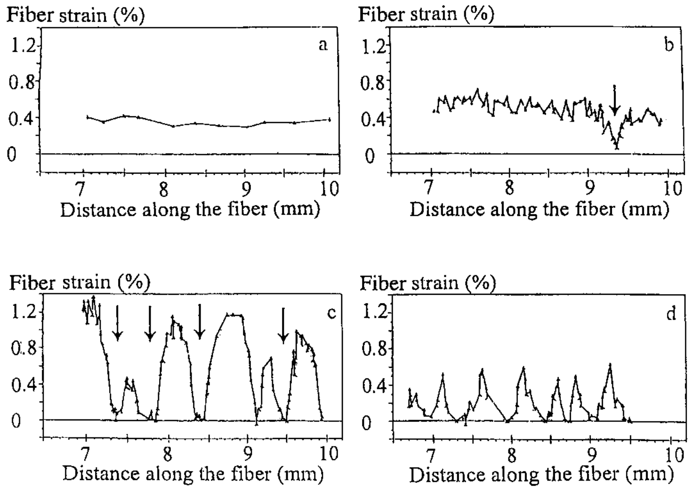

Fig. 3 Fiber strain measured by laser Raman spectroscopy during a microfragmentation test (applied strain: a 0.6, b 0.8, c 1.5, d 3.0 %)

Figure 3, obtained by Galiotis [13] by operating on the system Toray M40 sized fiber, Narmco 5250-2 BMI, and Ciba LY556-HT972 epoxy shows the fiber strain as a function of the distance of the examined points from the origin of the chosen fragmentation gauge length. At low mean strain, the local strains are uniformly distributed over x (Fig. 3a); when the applied mean strain increases, the first fracture is induced (Fig. 3b) but the local damage does not influence significantly the strains of the other points of the fiber and does not affect the stress increase borne by the rest of the fiber due to the increased elongation. Going on in increasing the mean strain, other fractures arise until saturation is reached; the strains in different fragments remain high in their central parts but are strongly reduced in the places where new fractures are formed (Fig. 3c). After saturation going to higher applied strains, all the fiber fragment strains are strongly reduced (Fig. 3d): this is mainly attributed to the interface damage (debridging).

By examining the $\varepsilon(x)$ profile around a fracture, it is possible to calculate the corresponding ISS (τ) distribution along x. The maximum value of the derivative of the function $\varepsilon(x)$ corresponds to the maximum of τ. The maximum ISS at low $\bar{\varepsilon}$ is normally at the fragment ends (Fig. 4), which agrees with the Cox equation. Beyond a certain applied strain (over 1.5 %), however, the maximum of ISS appears away from the fiber fragment end and shifts towards the middle of the fragment on increasing the applied strain. All the ISS maxima named IFSS data are averaged on all the fragments at each applied strain and their mean value is calculated as a function of strain (Fig. 5). The average maximum of ISS goes down when, increasing the applied elongation, interfacial debridging takes place. The maximum value of IFSS before debonding results which is somewhat above that calculated by the Kelly-Tyson microfragmentation method at saturation (which is a mean value).

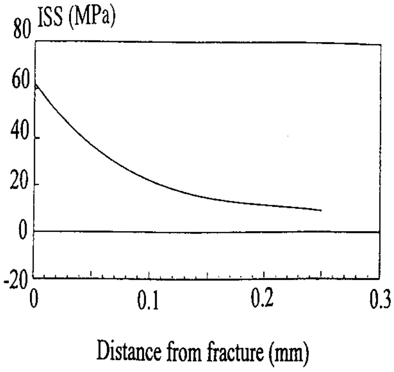

Fig. 4 Shear stress distribution at the fiber – matrix interface (applied strain 1.2 %)

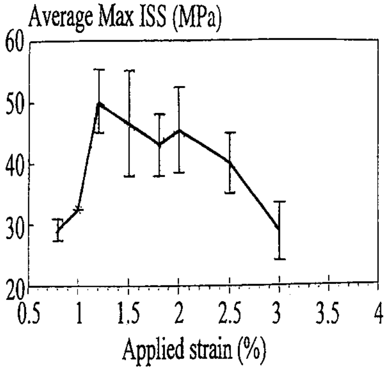

Fig. 5 IFSS as function of applied strain during SFC tests

Obviously, operating by LRS, the Kelly-Tyson calculation of τ_{ad} can be obtained by measuring the average fragment length, $\bar{l}$, by calculating l_c and by using for σ_{bf} the proper value obtained by the Weibull equation. The comparison gives IFSS = 46.6±8.7 MPa and τ_{ad} = 38 MPa [13].

The LRS method is able to evidence the debonded length of each fragment where ISS is zero. Figure 6 shows that these lengths increase with the applied strain, initiate at 1.5 % strain and involve 5 % of the fiber length.

Fracture shape and energetic aspects of SFC test

The shape of the fracture observed in polarized light in transparent systems during and after the tensile tests can clarify the failure mechanism at least in a qualitative way. Figure 7 shows examples of [14]:

(a) well developed stress field around the fiber breaks, which demonstrates an efficient shear mechanism of load transfer;

(b) fiber break and cone- or disk-shaped failure in the matrix, close to the fiber ends;

(c) easy debonding.

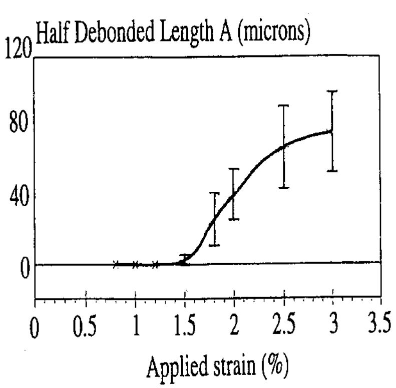

Fig. 6 Debonding length as function of applied strain during SFC tests

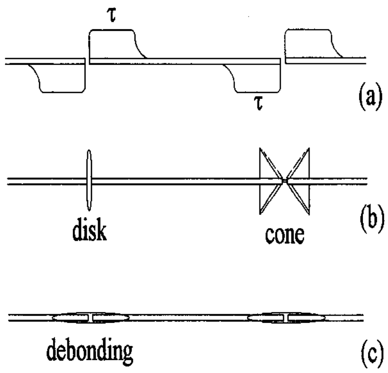

Fig. 7 Schematic of possible interface failure mechanisms

Table 2 shows the relation between the bond type, strength and the mechanism of fracture in cases (b) and (c).

Table 2 Relation between modes of failure and failure mechanisms

Type of failure	Properties
Failure starting even at low strains from filament ends in a strong matrix develops: - disk-shaped crack - two inclined conical cracks - both or none, shear strains evident	High bond strength
Failure starting from filament ends in a weak or soft matrix develops: - inclined conical cracks in the matrix	Bond strength sufficient to load filament by transfer
Shear stress pattern shifts toward filament center during loading. Friction stresses may act in the debonded region.	Bond strength not sufficient to load the filament to fracture.

To better understand the results obtained by the SFC test, one can take into consideration the energy involved in fracture in different components and in the region of the interface. Experimental observations show that when failure occurs, considering an instantaneous constant strain ε, the total elastic energy of the system ($U_{\mathrm{m}} + U_{\mathrm{f}}$) is at least in part spent in different possible ways, which are mainly:

(1) fiber cracks formation ΔU_{fb};

(2) formation of cracks in the matrix (disk-shaped or conical surfaces starting generally from both ends of the broken fiber) (ΔU_{mb});

(3) debonding energy associated with an interface or interphase rupture running around the fiber surface (ΔU_{deb});

(4) energy release in vibrations and viscoelastic dissipations (ΔU_{d}).

The mechanical energy balance when no external work is applied is expressed by

$$-\Delta(\mathrm{U_f}+\mathrm{U_m})=\Delta\mathrm{U_{deb}}+\Delta\mathrm{U_{fb}}+\Delta\mathrm{U_{mb}}+\Delta\mathrm{U_d} \tag{8}$$

where U_f and U_m are the elastic energies of fiber and matrix and the other ΔU are defined above in an explicit way. Some of these terms can be expressed rather easily.

(1) We try now to express ΔU_f taking into consideration a fragment length l_0 of the fiber under stress σ_{bf} (Fig. 8).

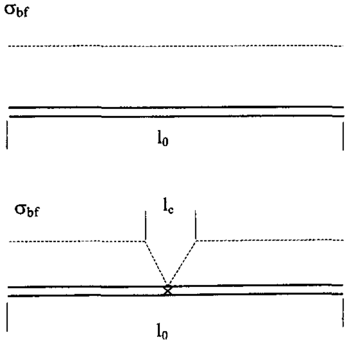

Fig. 8 Variation of stress distribution in a broken fiber

After the break, two fragments are generated. The system is now characterized by segments of length $l_c/2$ and segments of length (l_0-l_c) which remain in the same stress conditions as before. The elastic energy of the fiber segment (length l_0) before break is

$$U_f^0=\frac{1}{2}\sigma_{bf}\varepsilon_{bf}\left(\frac{\pi d_f^2}{4}l_0\right)=\frac{1}{2}\frac{\sigma_{bf}^2}{E_f}\frac{\pi d_f^2}{4}l_0 \tag{9}$$

The final energy of the undisturbed zone is

$$U_f'=\frac{1}{2}\frac{\sigma_{bf}^2}{E_f}\frac{\pi d_f^2}{4}(l_0-l_c) \tag{10}$$

For our considerations the energy state of reference is zero when $\sigma = 0$. The energy present in the two newly broken fiber ends is

$$U_f''=\frac{1}{3}\frac{\sigma_{bf}^2}{E_f}\left(\frac{l_c}{2}\right)\frac{\pi d_f^2}{4} \tag{11}$$

In fact the expression for U_f'' (elastic energy in the critical length of the fragments) related to one fiber fracture is obtained using the hypothesis that τ is a constant in the range $0 \le x \le l_c/2$ so that the behaviour of stress and strain is linear with respect to x. The equations are:

$$\sigma(x)=2\frac{\sigma_{bf}}{l_c}x \tag{12}$$

$$\varepsilon(x)=\frac{\sigma(x)}{E_f}=\frac{2\sigma_{bf}}{E_f l_c}x \tag{13}$$

The energy $\mathrm{d}U_f''/2$ accumulated in each fragment end at a distance x from the origin in the volume element $\mathrm{d}V = \mathrm{A}\,\mathrm{d}x$ is

$$\frac{\mathrm{d}U_f''}{2}=\frac{1}{2}\frac{\sigma^2(x)}{E_f}\mathrm{d}V=\frac{\pi d_f^2}{2E_f}\frac{\sigma_{bf}^2}{(l_c)^2}x^2\,\mathrm{d}x \tag{14}$$

Integrating (for the two fragments),

$$U_{\mathrm{f}}'' = -\frac{\pi d^2}{E_{\mathrm{f}}}\frac{\sigma_{\mathrm{bf}}^2}{(l_{\mathrm{c}})^2}\frac{\left[x^3\right]_0^{(l_{\mathrm{c}}/2)}}{3} = \frac{1}{3}\frac{\pi d_{\mathrm{f}}^2}{4}\frac{l_{\mathrm{c}}}{2}\frac{\sigma_{\mathrm{bf}}^2}{E_{\mathrm{f}}} \tag{15}$$

Finally,

$$-\Delta U_{\mathrm{f}} = U_{\mathrm{f}}^0 - \left(U_{\mathrm{f}}' + U_{\mathrm{f}}''\right) = \frac{l_{\mathrm{c}}}{3}\frac{\pi d_{\mathrm{f}}^2}{4}\frac{\sigma_{\mathrm{bf}}^2}{E_{\mathrm{f}}} \tag{16}$$

i.e.,

$$-\frac{\Delta U_{\mathrm{f}}}{U_{\mathrm{f}}^0} = \frac{2}{3}\frac{l_{\mathrm{c}}}{l_0} \tag{17}$$

This fiber energy decrement associated with fracture according to Eq. (8) is balanced by the energy spent by the different ΔU_i whichever is possible.

For example at low mean strains, if matrix and interface are strong, an increment of ΔU_{m} is mainly expected, as shown by the strong effects in polarized light due to shear stresses which are evidenced around the fragment ends. At higher strains, we observed that debonding may appear; the stress σ in the fiber observed by LRS becomes lower and interfacial shear stress is around zero demonstrating a failure of the interface. A complete study of energy partition can be done at low strains by using the finite element elastic model of the SFC test [14].

A complete observation of all the sample points is required to look at all the failure steps; simultaneous recording of stress, strain, and work is also needed to discover the values of different ΔU_i and the related stresses.

(2) Energy spent for the disk-shaped surface in the matrix (diameter D). Starting from the linear elastic fracture mechanic theory, we put $K_{\mathrm{IC}} = \sqrt{E\ G_{\mathrm{IC}}}$ where K_{IC} is the critical first-mode stress intensity factor at which fracture is propagated ($K = \sigma\sqrt{\pi a}$; a is the fracture initial length equivalent to the fiber diameter when fracture starts). Therefore

$$\frac{\pi D^2}{4}\frac{K_{\mathrm{IC}}^2}{E} = \Delta U_{\mathrm{b}} \tag{18}$$

In the case of a cone formation, $\Delta U_{\mathrm{bm}} = GA$ where A is the cone surface and G is in principle not the same G_{IC} because the fracture mode is not simply the first.

(3) The debonding energy can be expressed as

$$\Delta U_{\mathrm{deb}} = \overline{G}_0 \pi d_{\mathrm{f}} l_{\mathrm{deb}} \tag{19}$$

where $\overline{G}_0$ is the mean specific energy needed to detach the unit interphase surface and l_{deb} is the debonding length.

If τ is taken as a constant during the debonding (when we find a yield process at the interface), the force needed to detach the fiber is

$$F = \tau \pi d_{\mathrm{f}} l_{\mathrm{deb}} \tag{20}$$

Considering the energy variation due to the debonding advancement from x to x+dx, we get

$$\mathrm{d}U_{\mathrm{deb}} = \frac{F}{l_{\mathrm{deb}}} x \, \mathrm{d}x \tag{21}$$

By integrating we get

$$\Delta U_{\mathrm{deb}} = \tau \pi d_{\mathrm{f}} \int_0^{l_{\mathrm{deb}}} x \, \mathrm{d}x \tag{22}$$

i.e.,

$$\Delta U_{\mathrm{deb}} = \tau \pi d_{\mathrm{f}} \frac{l_{\mathrm{deb}}^2}{2} \tag{23}$$

Therefore the mean specific energy is

$$\overline{G}_0 = \frac{\Delta U_{\mathrm{deb}}}{\pi d_{\mathrm{f}} l_{\mathrm{deb}}} = \frac{\tau l_{\mathrm{deb}}}{2} \tag{24}$$

Effects of viscoelastic matrix on adhesion factor τ_{ad}

The pressure existing at the interface is one of the main factors which rule adhesion at different temperatures both in physical and chemical interphase bridging. Outwater suggested a simple relation valid in the debonding case, $\tau = \mu\sigma_{\mathrm{R}}$, where μ is a friction coefficient. The radial stress σ_{R} can be calculated from different models on the basis of the composite geometry. For a single continuous cylindrical inclusion, as in the SFC test before breaks, the Nairn model [15] can be used; a simplified expression gives [16]

$$\sigma_{\mathrm{R}} = \frac{(\alpha_{\mathrm{m}} - \alpha_{\mathrm{f}}) \cdot \Delta T \cdot E_{\mathrm{m}}}{1 + \nu_{\mathrm{m}} + (1 - \nu_{\mathrm{f}}) \frac{E_{\mathrm{m}}}{E_{\mathrm{f}}}} \tag{25}$$

which becomes

$$\sigma_{\mathrm{R}} \approx (\alpha_{\mathrm{m}} - \alpha_{\mathrm{f}}) \cdot \Delta T \cdot \frac{E_{\mathrm{m}}}{1 + \nu_{\mathrm{m}}} \tag{26}$$

in the case $E_{\mathrm{f}} >> E_{\mathrm{m}}$.

These expressions show that pressure depends on the difference between the mean dilatation coefficient of matrix (α_{m}) and of fiber (α_{f}), on the temperature variation ΔT after the molding or curing, and on the elastic properties (E_{m}, E_{f}, ν_{m}, ν_{f}) of the components.

In the case of polymer matrices, properties E_{m} and ν_{m} are functions of temperature and time. Therefore calculations of stresses must take into consideration their viscoelastic behaviour. This is done first of all by constructing master curves $E(t)$ and $\nu(t)$ or $G(t)$ at a reference temperature T_0 and the shift factors $a_{T_0}^{T}$. The master curve gives the proper modulus at T_0 as a function of a reference time ζ defined as

$$\zeta = \frac{t}{a_{T_0}^{T}} \tag{27}$$

With the master curve, the relaxation modulus can be evaluated in any condition if the cooling history $T(t)$ is known. Pressure can be therefore calculated according to Nairn or by Eq. (25).

Procedure of stress calculation at the interface

Let us start with cooling from a reference temperature T_r at which thermal stresses are considered to be zero. For a thermoplastic, one may assume $T_r = T_g$ for amorphous polymers and $T_r = T_m$ for crystalline polymers. For thermoset, the cure temperature may be taken as T_r. It is convenient to split the total temperature difference T_r-T into small equal steps ΔT_j (j =1, 2, ... u). In the SFC, for each ΔT_j, we get a radial contraction Δr_j which generates the corresponding $\Delta\sigma_j$ relaxing according to the matrix viscoelastic behaviour. E_m and ν_m values are found on the master curves as functions of the reference time ζ. A simple example illustrating the calculation procedure is shown in Fig. 9 (three cooling steps).

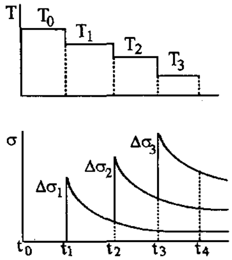

Fig. 9 Schematic of the cooling process

At time t_4 are present the three stresses $\Delta\sigma_1(t_4)$, $\Delta\sigma_2(t_4)$, $\Delta\sigma_3(t_4)$ generated, respectively, at times t_1, t_2, t_3 and relaxed in the time intervals t_4-t_1, t_4-t_2, t_4-t_3. The calculation program which solves the Nairn model equations is used to calculate the radial stress $\Delta\sigma_3$ (t_4) (and also the hoop and axial stresses).

This is done using the E_m and ν_m values obtained from the master curves at a reference time $\zeta_3 = \dfrac{(t_4 - t_3)}{a_{T_3}}$ and the expansion coefficients $\alpha_m(T_3)$. The next step is to calculate $\Delta\sigma_2$ (t_4), which was generated at time t_2, relaxed at T_2 during the reference time $\zeta_2 = \dfrac{(t_3 - t_2)}{a_{T_2}}$ and subsequently relaxed at T_3 during the reference time ζ_3. The Nairn equations are solved again using E_m and ν_m obtained from the master curves at the reference time $\zeta_2+\zeta_3$ and the proper α_m. Analogously it is possible to calculate $\Delta\sigma_1(t_4)$ making reference to E_m and ν_m valid for $\zeta_1+\zeta_2+\zeta_3$ where $\zeta_1 = \dfrac{(t_2 - t_1)}{a_{T_1}}$.

The total stress at the final time of observation (t_u) on the basis of the superposition principle is in general

$$\sigma(t_u) = \sum\nolimits_j \Delta\sigma_j(t_u - t_j) \tag{28}$$

The example of Fig. 10 shows σ_R at the interface of the system CF-PEI resin of a SFC sample, calculated using the Nairn model assuming an elastic behaviour of the fiber and a viscoelastic behaviour of the PEI matrix (for cooling rates of 10 and 1 °C/min). For comparison, the behaviour of the elastic matrix and the elastic fiber is also shown.

Different master curves of thermosets such as bismaleimide (BMI) and epoxy matrices and of thermoplastic polymers, both amorphous such as PEI and crystalline such as PEEK were prepared by our group and were used for these calculations [3,17]. The calculations give an important information on the radial stress entity but experimental check of the σ_R is not yet feasible at present. However, the importance of thermal stress relaxation on adhesion can be shown, for example, by the critical lengths measured at room temperature for the epoxy DGEBA-IPDA and PEI with high-tenacity carbon fibers (XAS), cooled down at different cooling rates [3]. It appears clearly (Fig. 11) that high cooling rates bring shorter l_c and higher τ_{ad}; this agrees with our relaxation model which shows that higher interface pressures and

τ_{ad} (Eq. (25) are reached at higher cooling rates (Fig. 10).

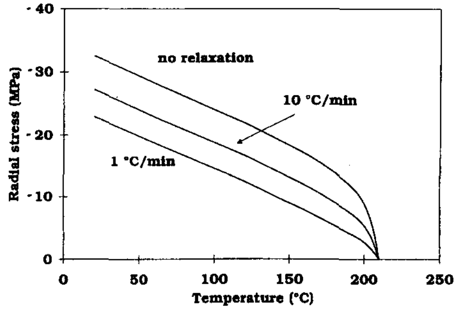

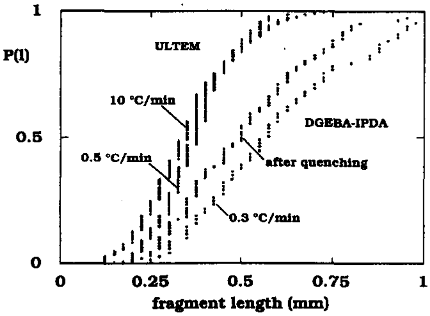

Fig. 10 Radial residual stress at the PEI/XAS interface as function of the end cooling temperature

Fig. 11 Fragment lengths observed in epoxy/XAS and PEI/XAS SFC tests after coling at different rates

Equation (25) indicates that pressure at the interface must decrease by increasing the temperature for two reasons: the first is that factor ΔT is reduced, the second is that the modulus decreases on increasing T. SFC tests made at higher than room temperatures in fact show a regular decrease in τ_{ad} both for thermoplastic and thermoset resins. Figure 12 shows the behaviour of the thermoplastic ULTEM (amorphous) and PEEK (semicrystalline) in contact with the same carbon fiber (Courtalds XAS). It can be seen that in thermoplastic matrices, adhesion goes remarkably down with increasing temperatures and reaches a negligible value for temperatures approaching the T_g (amorphous polyetherimide ULTEM) and T_m in the case of PEEK (T_g = 143 °C, T_m = 334 °C). Epoxy matrices (CIBA LY556 + HT972 and DGEBA-IPDA) with different carbon fibers (Toray M40 and Courtalds XAS) show a strong decrease of adhesion on increasing T but, in correspondence with the cure temperature (140 °C) and even above, a residual adhesion is maintained.

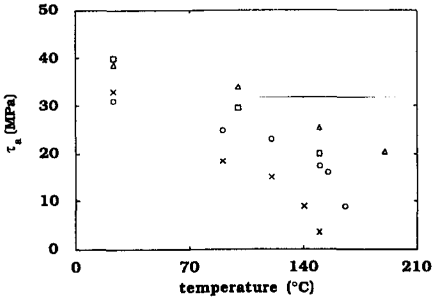

Fig. 12 τ_{ad} as function of temperature in different composite systems (□ ULTEM-XAS, Δ PEEK-XASO, O LY556/HT972-M40, X DGEBA/IPDA-XAS)

The presence of a consistent value of $\tau = \tau_c$ at 140 °C is an indication of the existence of a chemically bonded structure which should be independent of temperature. The difference $\tau_{ad} - \tau_c$ therefore should be attributed to physical effects and mainly to the pressure generated by the different thermal strains of matrix and fiber and by the Poisson effect. The last one gives a contribution to pressure given [16] by

$$\sigma_{\mathrm{RP}} = \frac{\varepsilon(\nu_{\mathrm{m}} - \nu_{\mathrm{f}})}{\left[\frac{(1+\nu_{\mathrm{m}})}{E_{\mathrm{m}}} + \frac{(1-\nu_{\mathrm{fT}} - 2\nu_{\mathrm{fL}}^2)}{E_{\mathrm{fT}}}\right]} \tag{29}$$

where ν is the Poisson coefficient; subscripts m and f refer to matrix and fiber; L and T indicate longitudinal and transversal directions.
An estimate for an epoxy-CF system shows that σ_{RP} at 25 °C is about 30 % of the total σ_R [18].

Extension of the SFC method to brittle matrices
When the matrix is so brittle that the strain-at-break of the matrix is lower than the fiber break strain, $\varepsilon_{bm} < \varepsilon_{bf}$, the fiber-fracturing process generating fragments cannot take place and no critical length can be measured. A case of our recent interest was that of BMI (Narmco 5250-2, BASF) (ε_r = 1.7%) used with high-tenacity carbon fibers, unsized TUS (ε_r = 1.9%). The general mechanical properties of BMI and fibers are reported in Table 3.

Table 3 Mechanical properties of matrices and fibers

Quantity (unit)	BMI	Epoxy (LY556-HT972)	TUS	MUS	XAS
σ_r (MPa)	69	65	~ 5000	~ 3000	4500
E (GPa)	3.8	2.4	260	330	230
ε_r (%)	~ 1.7	> 5 %	~ 1.9	~ 0.9	~ 1.9

A fragmentation method applied to a three-phase monofilament named coaxial SFC, useful to get shear adhesion stress τ_{ad}, was first suggested by Jacques and Favre [19]. It is mainly useful for comparing the efficiency of different adhesives with the same adherent. They proposed to coat the fiber with a thin sheath of the brittle resin (BMI) and to embed the coated fiber into a ductile resin (epoxy) which maintains the specimen integrity during the tensile test (Fig. 13).

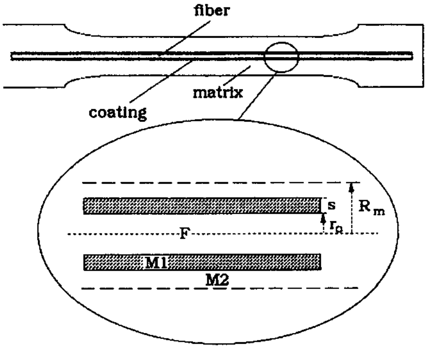

Fig. 13 Geometry of the coaxial single fiber composite coupon

When the brittle resin sheath M1 is broken, the load becomes shared between the fiber F bound to M1 and the tough resin M2 until the fiber is broken somewhere on increasing the load. At this moment, the load exchange between the tough matrix and the fiber end is obtained, as usual, by the shear stress transfer which is transmitted through the tough and the brittle resins to the fiber. In this way, fragmentation can take place but the failure mechanical study is quite difficult. We suppose that shear yielding or debonding should happen more probably at the interface F/M1.

Stress, strain and shear energy analysis of a system made by a continuous fiber embedded in a matrix with or without an intermediate sheath can be done according to the mechanics of continuous elastic systems [15, 17]. With a computer program, different failure criteria in any point of the system can be checked by a relative comparison of the local values with the possible limit values of materials and interfaces. In our case, the highest values of von Mises stress, of the strain energy density W_E and of the distortion energy density W_D, are found at the interface between fiber and BMI (Fig. 14). The stress calculation was done from the data of Table 3 for a load of 50 MPa and a cooling range ΔT of -120 °C.

The introduction of the BMI interlayer considerably reduces radial stresses (σ_R) and tangential stresses (σ_T) in the outer epoxy matrix in comparison with the stresses acting in the same epoxy in the absence of BMI (Fig. 15), when the matrix touches the fiber. We observe that the application of the external load increases the stresses σ_R and σ_T of thermal origin at both the interfaces F/M1 and M1/M2. In conclusion, according to the calculations, the first break in a continuous system should occur in the brittle resin starting at the interface F/M1. After that the load increment on the fiber can soon cause the fiber fracture. Crack propagation in the matrix M1 is stopped at the tough resin interface. It was observed [19], for example in the case of TGDDM (Narmco 5208) and the high-tenacity CF, that fractures in the brittle matrix have a penny-like shape. The load transfer involves shear stresses through the interfaces M2/M1 and M1/F. In this way, the fiber can be re-stressed, new fiber breaks appear and more energy per unit volume is released. In proper conditions, this may also cause the failure at the fiber-BMI interface (debonding). Our observations under an optical microscope show that in our case (TUS fiber/BMI/LY556 + HT972), both microfragmentation and debonding of the fiber occur while the sheath remains steady in the matrix. We can conclude that, in our case, Eq. 3 can be used to calculate τ_{ad} of the fiber as a good means to assess interface properties even if this value is the result of combination of two different processes of shear transfer.

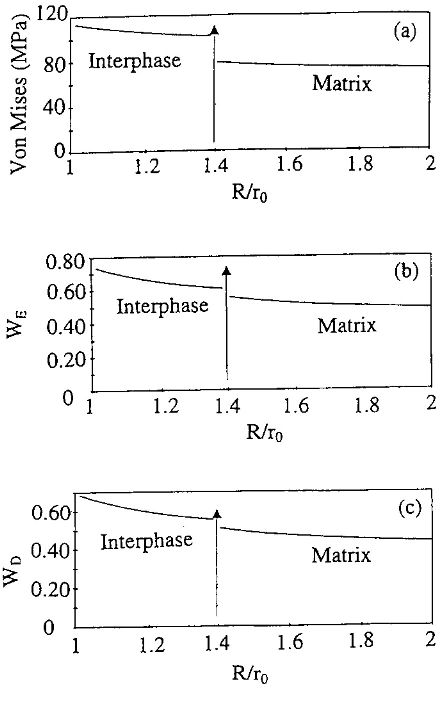

Fig. 14 Comparison of failure criteria in a CF/BMI epoxy system

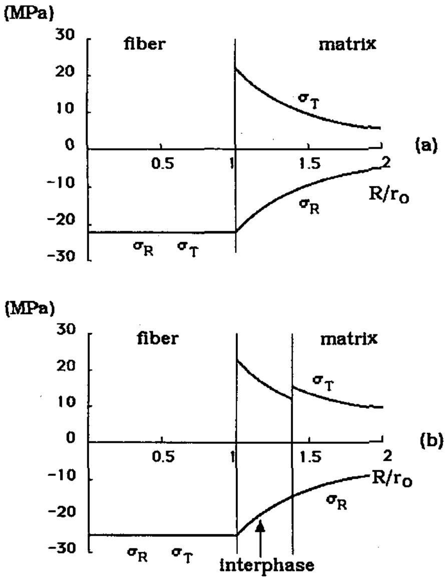

Fig. 15 Stress distribution in a CF/epoxy system with and without a BMI interphase

According to the Cox model [8], the shear stress at the fiber interface embedded in a monophasic matrix is

$$\tau = \frac{E_f \varepsilon \beta \sqrt{\frac{A_f}{4\pi}} \sinh \beta \left(\frac{1}{2} - x \right)}{\cosh \frac{\beta l}{2}} \tag{30}$$

where

$$\beta = \sqrt{\frac{G_m}{E_f} \frac{2\pi}{A_f \ln \frac{R_m}{r_0}}} \tag{31}$$

R_0 and R_m are the fiber and the equivalent matrix radii, respectively. When a two-phase matrix is present, we propose as a first approximation and very roughly, to substitute for G_m the equivalent modulus G_c of the series combination of the two matrices. G_c is found by applying the equation

$$\frac{1}{G_c} = \frac{\phi_1}{G_1} + \frac{\phi_2}{G_2} \tag{32}$$

where ϕ_1 is the volume fraction of the brittle phase M1 and ϕ_2 is the complementary fraction of the tough phase M2.
By simple geometric considerations,

$$\phi_1 = \frac{s(2r_0 + s)}{(R_m^2 - r_0^2)} \tag{33}$$

We can therefore calculate from Eqs. (30) and (31) τ_c, which should represent the effective mean adhesion. If the adhesion of fiber with the brittle matrix alone is to be evaluated, Eqs. (30) and (31) should be used employing G_1 modulus for G_m, thus obtaining τ_a. For the ratio τ_a / τ_c, one obtains

$$\frac{\tau_a}{\tau_c} = \frac{\beta_a}{\beta_c} \frac{\sinh \beta_a \left(\frac{1}{2} - x \right)}{\sinh \beta_c \left(\frac{1}{2} - x \right)} \frac{\cosh \frac{\beta_c l}{2}}{\cosh \frac{\beta_a l}{2}} \approx \frac{\beta_a}{\beta_c} \tag{34}$$

where

$$\frac{\beta_a}{\beta_c} = \sqrt{\frac{G_1}{G_c}} \tag{35}$$

Therefore τ_a should be higher than the τ_c of the composite model.

In conclusion, the experimental SFC τ_a evaluated by the Kelly-Tyson method using a two-phase matrix appears to correspond to the composite model and therefore underestimates the effective adhesion coefficient τ_a between the brittle component alone and fiber.

$$\frac{\tau_a}{\tau_c} = 1.195$$

An example of the application of the modified SFC method in our recent studies of adhesion to the system with high-tenacity and high-modulus carbon fibers (T800 and M40) and BMI Narmco 5250-2 embedded in epoxy Ciba LY556+HT972 is shown. In our case G_1 = 1.62 GPa, G_2 = 1.04 GPa, G_c = 1.13 GPa, r_0 = 3.3 μm, s = 1 μm, ϕ_1 = 23.2 % and τ_a/τ_c = 1.195. ϕ_1 was calculated by Eq. (33) with $R_m = 2r_0$.

Recent results

We are presenting some recent results reached in the study of a BMI resin and unsized high-tenacity (TUS) and high-modulus (MUS) carbon fibers. The fibers have an imperfect graphitic structure with many oxygen groups and a low hydrogen content which enable the chemical bonding of modifiers on the CF surface. The selected modifiers can react with BMI resins. Based on the classical physico-chemical description of the carbon fiber surface, the reactions used in surface modification are Diels-Alder cycloaddition and nucleophilic substitution.

Diels-Alder reaction is typically carried out with conjugated dienes and olefins containing electron-withdrawing groups. The reaction does not occur if the diene structure is a part of a perfectly conjugated system such as benzene, but occurs if the diene is a part of polyconjugated ring systems [20]. In this case π electrons are more weakly bonded than in benzene, so that they can react with dienophiles such as tetracyanoethylene (TCNE), maleic anhydride (MA) and citraconic anhydride (CA).

The presence of hydroxy groups in the imperfect graphitic systems of carbon fibers can be used for their surface modification with bases such as ammonia and amines. The exchange reaction of OH group for amino group is not easy with phenol, but proceeds easily in polycyclic compounds containing more than four rings [21].

Both types of the reactions occur in the case of high-tenacity (TUS) and high-modulus (MUS) unsized fibers, but the different types and structures of MUS and TUS have a certain influence on the conversion. The MUS fiber reveals a higher order in microcrystalline graphitic structure than TUS due to the higher heat treatment temperature used in the fiber production starting from PAN precursors. We found by ESCA analysis that MUS fibers react with NH_3 reaching higher conversions of nucleophilic substitions than TUS under equal conditions.

Adhesion evaluation was done by the SFC test. Due to the low strain-at-break of BMI, all the adhesion tests were done using the coaxial SFC method. The fibers coated with BMI were embedded after a first cure in epoxy Ciba LY 556 + HT 972 and cured at 140 °C. Table 4 summarizes the results of l_c at room temperature in relation to the type of the treatment, both in the case of TUS and MUS fibers.

We can see that the shortest critical length l_c was obtained in the case of TUS treated with ammonia at room temperature (l_c = 0.39 mm). Quite similar results are obtained with MUS fibers (minimum l_c= 0.37 with NH3), while the Diels-Alder treatment in this case gave higher l_c.

Table 4 Micromechanical results of T800 and M40 fibers/BMI/epoxy LY556-HT972 systems with different fiber treatments

Fiber	Sample	Reactant(s)[a]	Time/temperature (h/°C)	l_c (mm)
T800	101	ammonia	120/room	0.39
	66	ammonia	9/130	0.50
	112	ammonia	9/140	0.44
	3	40% MA+1% DCP	6/150	0.43
	30	50% MA+1% DCP	12/150	0.53
	62	50% MA	6/150	0.43
	31	CA + DCP	12/150	0.49
	0	as received (unsized or sized)	-	0.43
M40	88-108	ammonia solution	120/room	0.41
	11B-19B-	ammonia vapor	9/130	0.45-0.49
	74	ammonia vapor	15/130	0.37
	10C	TCNE	7/room	0.65
	5B	100% AA + BPO	10/80	0.55
	17B	EDTA + DCP	5/140	0.57
	13B	as received unsized	-	0.75
	1B	extracted	-	0.65
	75-2B-20B -	as received epoxy-sized	-	0.65

[a] MA maleic anhydride, DCP dicumyl peroxide, TCNE tetracyanoethylene, CA citraconic anhydride, AA acrylamide, BPO dibenzoyl peroxide

Figure 16 shows the dependence of l_C versus the nitrogen surface content of the treated TUS and MUS fibers. Nitrogen is not present in the MUS surface and therefore its presence is exclusively due to the bound ammonia molecules. It can be observed that in our cases, ammonia treatment is the most efficient way for increasing the adhesion between BMI and fiber. In fact, treatment with other nitrogen-containing compounds of higher MW have given higher l_C.

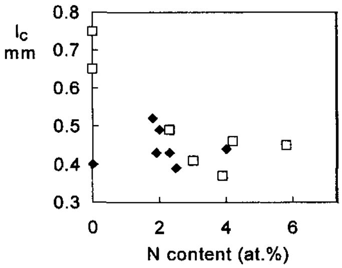

Fig. 16 Critical length measured on treated fibers with different surface nitrogen concentrations (□ M40, ◆ T800)

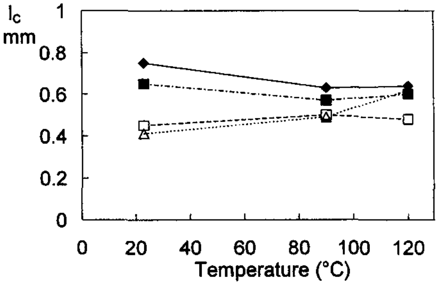

Fig. 17 Critical length of ammonia treated M40 fibers as function of temperature (◆ MUS, ■ MEBS, □ M40-11B, Δ M40-88/108)

Various tests were done to check the dependence of l_c versus T between room temperature and 120 °C. This upper limit is due to the low modulus of the embedding epoxy resin, which makes difficult to compare the results obtained at different temperatures. On increasing the test temperature, l_c increases and τ decreases.

Figure 17 shows the behaviour of the NH_3-treated MUS - BMI systems in dependence on temperature: it is interesting to observe that while no remarkable variation of adhesion is detected in TUS fibers after the treatment, MUS as such and even a commercial epoxy-sized M40 fiber (MEBS) appear to be characterized by a lower adhesion to BMI than ammonia-modified MUS.

Preparation of fiber tows impregnated with a BMI 5250-2 resin dissolved in acetone (50%) can be done by eliminating the solvent and curing the resin. The tows were submitted to tensile test at different temperatures. While the break load does not change on increasing temperature, due to the carbon fiber presence, the pull-out length distribution of the broken fibers can be studied on tows tested at different temperatures.

The length distribution at 20 and 250 °C is wide and the average length increases notably from 17.8 to 34 μm. At the moment, no reliable calculation can be done on these data to obtain the adhesion shear resistance.

At the highest temperature (250 °C), the radial stress given by Eq. 25 should be positive (tensile). Adhesion under this condition (250 °C) could be only due to chemical bonds existing at the interface or simply to the viscous drag motion between fiber and polymer network if the interface chemical bonds are at least partially effective.

REFERENCES

1. M.R. Piggot (Ed.), *Interfaces in Composites*, Elsevier 1991.
2. J.P. Favre, M.H. Auvray, P. Cheneau-Henry, C. Galiotis, C. Vlattas, A. Paipetis, M. Pegoraro, F. Severini, L. Di Landro, L. Yuan, *Polym. Compos.* 17, 936 (1996).
3. L. Di Landro, M. Pegoraro, *Composites* 27A, 847 (1996).
4. L. Di Landro, M. Pegoraro, *Chim. Ind*, 70(6), 86 (1988).
5. L. Di Landro, M. Pegoraro, *J. Mater. Sci.* 22, 1980 (1987).
6. M. Pegoraro, L. Di Landro, *Makromol. Chem., Macromol. Symp.* 70/71, 193 (1993).
7. A. Kelly, *Strong Solids*, Clarendon Press, Oxford 1973.
8. H.L. Cox, *Br. J. Appl. Phys.* 3, 72 (1952).
9. W. Weibull, *J. Appl. Mech. (ASME)* 18, 293 (1951).
10. A. Kelly, W.R. Tyson, *J. Mech. Phys. Solids* 13, 329 (1965).
11. C. Galiotis, in *Interfaces in Composites* (M.R. Piggot, Ed.), Elsevier 1991, p. 125.
12. A. Paipetis, C. Galiotis, *Composites* 27A, 755 (1996).
13. BREU CT 91-503, *Interface Contribution to the Temperature Dependent Properties of Carbon Fiber Reinforced BMI Composites*. Report 1993.
14. A.T. DiBenedetto, in *Interfaces in Composites* (M.R. Piggot, Ed.), Elsevier 1991, p. 103.
15. J.A. Nairn, *Polym. Compos.* 6 ,123 (1985).
16. L. Di Landro, A.T. DiBenedetto, J. Groeger, *Polym. Compos.* 9, 209 (1988).
17. F. Crescenti, C. Salvetti, M.S. Thesis, Politecnico di Milano, 1994.
18. S. Schutt, Ph.D. Thesis, Inst. für Kunststoffverarbeitung (IKV) and Politecnico di Milano, 1995.
19. J.P. Favre, D. Jacques, *J. Mater. Sci.* 25, 1373 (1990).
20. J. March, *Advanced Organic Chemistry*, 4th ed., J. Wiley 1992, p. 841.
21. L.F. Fieser, *Advanced Organic Chemistry*, Reinhold 1961, p. 889.